Exciton dissociation at donor-acceptor polymer heterojunctions: quantum nonadiabatic dynamics and effective-mode analysis

Hiroyuki Tamura,[1] Eric R. Bittner,[2] and Irene Burghardt[1]

[1]*Département de Chimie, Ecole Normale Supérieure,*
24 rue Lhomond, F–75231 Paris cedex 05, France
[2]*Department of Chemistry and Texas Center for Superconductivity,University of Houston, Houston, Texas 77204*
(Dated: February 6, 2008)

The quantum-dynamical mechanism of photoinduced subpicosecond exciton dissociation and the concomitant formation of a charge-separated state at a TFB:F8BT polymer heterojunction is elucidated. The analysis is based upon a two-state vibronic coupling Hamiltonian including an explicit 24-mode representation of a phonon bath comprising high-frequency (C=C stretch) and low-frequency (torsional) modes. The initial relaxation behavior is characterized by coherent oscillations, along with the decay through an extended nonadiabatic coupling region. This region is located in the vicinity of a conical intersection hypersurface. A central ingredient of the analysis is a novel effective mode representation, which highlights the role of the low-frequency modes in the nonadiabatic dynamics. Quantum dynamical simulations were carried out using the multiconfiguration time-dependent Hartree (MCTDH) method.

The photophysics of π-conjugated organic semiconductor systems is a key ingredient in the technological development of optoelectronic devices.[1] Due to their spatially extended structure, these systems exhibit both the molecular characteristics of their components and the collective electronic excitations (exciton states) characteristic of lattice structures. The coupling between electronic and nuclear motions results in the localization ("self-trapping") of exciton states, along with the coherent nuclear dynamics and vibronic coupling phenomena known from molecular systems.[2, 3, 4, 5, 6, 7, 8] Experiments have indeed provided evidence for coherent vibrational dynamics[9] and ultrafast (typically $\sim$ 100 fs) decay of electronic excitations.[10, 11]

Of particular interest are ultrafast exciton dissociation processes at polymer heterojunctions,[3, 4, 5, 11, 12, 13] comprising two materials with a ΔE off-set between the constituent valence and conduction bands (see Fig. 1). In molecular terms, this is the energy difference between the HOMO or LUMO levels of the two components. If ΔE is large compared to the exciton binding energy ϵ_B (for typical organic polymers, $\epsilon_B \approx 0.5$ eV), the photoexcited exciton state decays to an interfacial charge-separated state (or exciplex).[3, 4, 5, 11, 12, 13] Generally, such a situation is desirable for photovoltaic systems where ΔE provides the driving force for charge-separation upon photoexcitation. On the other hand, if $\epsilon_B > \Delta E$, the excitonic state is stable, and such situations are best suited for light-emitting diode (LED) applications. If $\epsilon_B \simeq \Delta E$, charge separation and exciton regeneration processes tend to compete.[11, 12, 13]

Even though considerable progress has been achieved over recent years in the electronic structure characterization of polymer semiconductor systems,[3, 5, 11] only tentative explanations have been given for the quantum-dynamical mechanism of the relevant charge transfer and decay processes.[3, 14] This applies, in particular, to the

electronically nonadiabatic decay channels which are of key importance for the ultrafast phenomena mentioned above. Given the presence of multiple electronic state crossings in conjunction with electron-phonon vibronic couplings, nonadiabatic crossing regions and conical intersection topologies are expected to play a landmark role. Against this background, this Communication aims to provide a detailed quantum-dynamical picture of the nonadiabatic events determining exciton dissociation and formation of a charge transfer (exciplex) state at a polymer heterojunction.

In the following, we focus upon the fate of the primary photo-excitation at a donor-acceptor heterojunction formed at the phase-boundary between poly[9,9-dioctylfluorene-co-N-(4,butylphenyl)diphenylamine] (TFB) and poly[9,9-dioctylfluorene-co-benzothiadiazole] (F8BT) when spin-cast from solution.[13, 15] The optimized molecular geometry of the two polymer chains at the interface is shown in Fig. 1. LEDs fabricated using these materials exhibit considerable luminescence intensity. This is remarkable because the relative HOMO energy off-set between the two polymers, ΔE, is only slightly larger than ϵ_B.[3, 4, 5, 11, 13] The photoexcited exciton (XT) state is thus only marginally stable against dissociation into a charge-transfer (CT) exciplex state, and the majority of the primary exciton population is indeed found to undergo charge separation.[13, 15] Although the CT state is weakly emissive, appearing 140 ± 20 meV to the red of the exciton, the considerable luminescence is attributed to secondary excitons formed by endothermic back transfer of the hole from TFB$^+$ to F8BT$^-$ to form the F8BT exciton with an activation energy of 100 ± 30 meV.[13, 15, 16]Nonadiabatic XT/CT state interactions clearly play a crucial role in this system.

In order to understand how nuclear motion influences the electronic transfer and decay mechanisms at
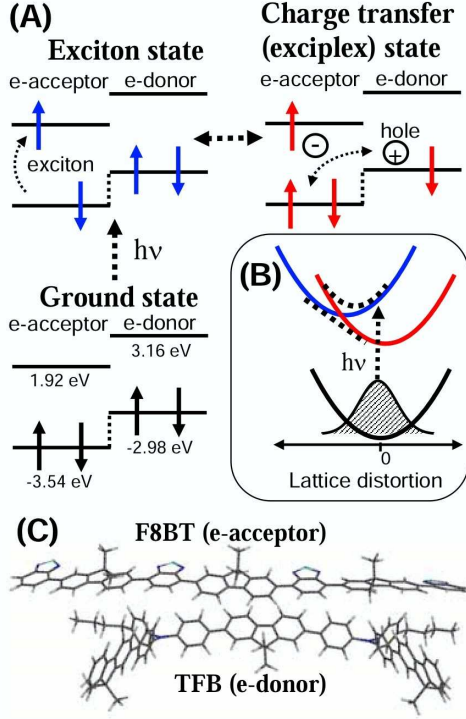
FIG. 1: (A) (Color online) Schematic diagram illustrating the electronic structure and photophysics of the TFB:F8BT donor-acceptor heterojunction. The solid and dashed lines indicate the energy levels and band offset ΔE, respectively; the solid arrows indicate the electron occupancies. (B) Simplified one-dimensional scheme of the photoexcitation and subsequent nonadiabatic potential crossing process. The black, blue and red curves indicate the ground, exciton and charge transfer states, respectively. The dashed lines indicate the adiabatic potentials at the avoided crossing. (C) Optimized molecular geometry, from density functional theory (DFT) calculations, of the parallel TFB and F8BT polymer chains at the heterojunction interface.

expected to carry over to a general class of conjugated polymer systems.

The following analysis makes extensive use of a recently developed effective-mode description of the nonadiabatic dynamics at conical intersections,[17, 18, 19, 20, 21] in conjunction with efficient multiconfigurational quantum propagation techniques.[22, 23, 24, 25] Our previous analysis has shown that the cumulative effects of many modes in a nonadiabatic coupling situation can be represented by *three effective modes* that entirely determine the short-time dynamics. In the present study, we further connect this previous analysis to a systematic, Mori-chain type decomposition of the phonon bath[26, 27] (see also the related development in Ref.[30]). As shown below, the explicit 24-mode phonon
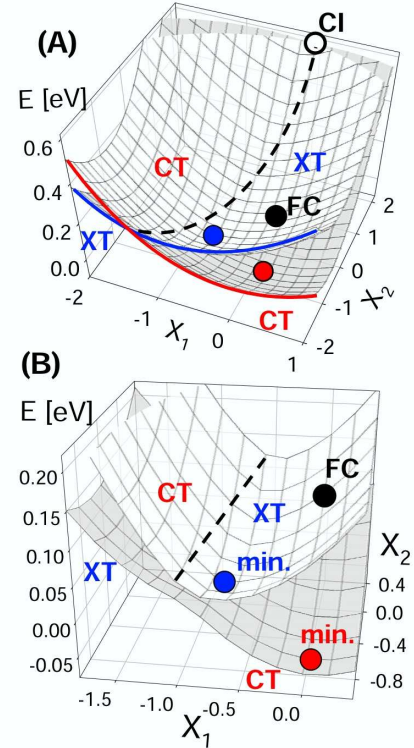

FIG. 2: (Color online) (A) Coupled adiabatic potential energy surfaces (PESs) as a function of the branching plane coordinates (X_1, X_2), and (B) zoom-in on the avoided-crossing region. The black, white, blue and red circles indicate the respective locations of the Franck-Condon (FC) geometry, the conical intersection (CI), and the minima of the exciton (XT) and charge transfer (CT) states, respectively. The blue and red lines indicate the XT and CT diabatic states, respectively. The dashed line indicates the XT-CT avoided-crossing seam line.

the TFB:F8BT heterojunction, we carried out quantum-dynamical simulations based upon the two-state vibronic coupling model put forward by one of us in Refs.[3, 14]. A subpicosecond scale decay from the XT state is induced by vibronic interactions involving high-frequency (C=C stretch) and low-frequency (torsional) modes. As explained below, we identify an extended nonadiabatic coupling region in the vicinity of a multi-dimensional intersection space. While the electron-phonon coupling is largely carried by the high-frequency modes, the low-frequency modes are shown to play a key role in the decay dynamics. The main features of this dynamics are

bath of the model under discussion can thus be replaced by a 9-mode effective bath over the time scale of interest.

Our starting point is the following electron-phonon Hamiltonian for the coupled XT and CT states interacting with an N-mode phonon bath,[14, 28]

$$\boldsymbol{H} \;=\; \boldsymbol{V}_\Delta + \sum_{i=1}^{N} \boldsymbol{H}_i$$

where

$$\boldsymbol{H}_i = \frac{\omega_i}{2}\left(p_i^2 + x_i^2\right)\mathbf{1} + \begin{pmatrix} \kappa_i^{(1)} x_i & \lambda_i x_i \\ \\ \lambda_i x_i & \kappa_i^{(2)} x_i \end{pmatrix} \quad (1)$$

with $p_i^2 = -\partial^2/\partial x_i^2$ and the electronic splitting $\boldsymbol{V}_\Delta = -\Delta\boldsymbol{\sigma}_z$ (with $\boldsymbol{\sigma}_z$ the Pauli matrix). Mass and frequency weighted coordinates were used, along with the convention $\hbar = 1$. As mentioned above, the phonon bath comprises a high-frequency branch composed of C=C stretch modes and a low-frequency branch of torsional modes. An explicit representation in terms of $N{=}24$ modes was introduced according to Ref. [14].

Eq. (1) corresponds to a general linear vibronic coupling form, in a diabatic representation,[28] and was parameterized by semiempirical calculations as described in Refs.[3, 5, 7]. The Hamiltonian Eq. (1) gives rise to an $(N-2)$-dimensional conical intersection space,[28] which is the key feature determining the nonadiabatic dynamics of the system. Indeed, the nonadiabatic decay induced by conical intersections is often ultrafast, i.e., occurring on a subpicosecond to picosecond time scale.

For the purpose of the following discussion, a decomposition of the phonon bath in terms of collective, or effective modes is introduced. To this end, we use an orthogonal coordinate transformation, $\boldsymbol{X} = \boldsymbol{T}\boldsymbol{x}$,[17, 18, 19, 20] leading to the following decomposition in terms of *effective* vs. *residual* modes,

$$\boldsymbol{H} = \boldsymbol{H}_{\mathrm{eff}} + \boldsymbol{H}_{\mathrm{res}} \quad (2)$$

with the part $\boldsymbol{H}_{\mathrm{eff}}$ which contains *three effective modes* (X_1, X_2, X_3) that entirely define the coupling to the electronic subsystem,

$$\boldsymbol{H}_{\mathrm{eff}} \;=\; \boldsymbol{V}_\Delta + \sum_{i=1}^{3}\frac{\Omega_i}{2}(P_i^2 + X_i^2)\,\mathbf{1} + \sum_{i,j=1,j>i}^{3} d_{ij}(P_iP_j + X_iX_j)\,\mathbf{1}$$
$$+ \sum_{i=1}^{3} K_iX_i\mathbf{1} + \begin{pmatrix} D_1X_1 + D_2X_2 & \Lambda X_1 \\ \\ \Lambda X_1 & -D_1X_1 - D_2X_2 \end{pmatrix} \quad (3)$$

Here, a topology-adapted representation[18] was chosen, where (X_1, X_2) lift the degeneracy at the intersection (and thus span the branching plane[29]), while X_3 lies in the intersection space. The modes (X_1, X_2) define a suitable reduced representation of the intersecting surfaces, as illustrated in Fig. 2. The parameters of Eq. (3) relate to the original Hamiltonian Eq. (1) as described in Refs.[18, 26].

The residual Hamiltonian $\boldsymbol{H}_{\mathrm{res}}$ contains the remaining $(N-3)$ modes, and their bilinear coupling to the effective modes and among each other,

$$\boldsymbol{H}_{\mathrm{res}} \;=\; \sum_{i=4}^{N}\frac{\Omega_i}{2}(P_i^2 + X_i^2)\mathbf{1}$$
$$+ \sum_{i=1}^{N}\sum_{j=4}^{N} d_{ij}\left(P_iP_j + X_iX_j\right)\mathbf{1} \quad (4)$$

Importantly, $\boldsymbol{H}_{\mathrm{res}}$ is diagonal with respect to the electronic subspace.

The transformation leading to Eqs. (2)-(4) introduces a hierarchical structure in the phonon bath: While the effective modes couple directly to the electronic two-level system, the residual modes couple in turn to the effective modes. The new choice of coordinates has important implications for possible approximations, since the effective mode Hamiltonian $\boldsymbol{H}_{\mathrm{eff}}$ by itself preserves the first three moments of the overall Hamiltonian.[19] Hence, the *short-time dynamics is entirely described by $\boldsymbol{H}_{\mathrm{eff}}$.*

The concept of a mode hierarchy can be carried further by introducing additional transformations within the subspace of residual modes. In particular, $\boldsymbol{H}_{\mathrm{res}}$ can be transformed to a band-diagonal form,[26] corresponding to a *hierarchy of residual bath modes* (see also Ref.[30] for a related analysis). An approximate nth-order, i.e., $(3+3n)$-mode Hamiltonian can be defined by truncating this hierarchy at a given order,

$$\boldsymbol{H}^{(n)} = \boldsymbol{H}_{\mathrm{eff}} + \sum_{l=1}^{n} \boldsymbol{H}_{\mathrm{res}}^{(l)} \quad (5)$$

with the lth order residual bath Hamiltonian

$$\boldsymbol{H}_{\text{res}}^{(l)} = \sum_{i=3l+1}^{3l+3} \frac{\Omega_i}{2}(P_i^2 + X_i^2)\boldsymbol{1}$$
$$+ \sum_{i=3l+1}^{3l+3}\sum_{j=i-3}^{i-1} d_{ij}\left(P_iP_j + X_iX_j\right)\boldsymbol{1} \qquad (6)$$

The results shown in Fig. 3, to be discussed in detail below, illustrate the effect of truncating the hierarchy of residual bath modes.

The scheme of Eqs. (5)-(6) corresponds to a generalized Mori chain, which can be shown to conserve successive orders of the Hamiltonian moments.[27] If truncated at a given order, the hierarchy can be formally closed by adding Markovian dissipation.[26, 27]

As can be inferred from the reduced representation of Fig. 2, in the (X_1, X_2) subspace, a conical intersection indeed exists in the present system, and an extended avoided crossing region is present in its vicinity. The figure further illustrates that the minima of both electronic states are located on the same side of an avoided-crossing seam that departs from the conical intersection. Following the terminology of Marcus theory, the system can thus be classified in terms of the "inverted regime".[3] Due to the prevalent weak coupling in the avoided-crossing region, the zeroth-order picture of the dynamics is expected to be markedly diabatic. With a Franck-Condon (FC) initial condition ($X_1 = X_2 = 0$), the wavepacket rapidly accesses the nonadiabatic coupling region, but does not directly encounter the conical intersection.

Fig. 3 (trace "exact") shows results of quantum-dynamical calculations for the overall 24-mode system according to the Hamiltonian Eq. (1), using the multiconfiguration time-dependent Hartree (MCTDH) method.[22, 23, 24, 25] From the figure, one can infer that the XT state population has decayed to about 50% after 200 fs, with a corresponding increase in the CT state population. Subsequent to the initial decay, the populations of the two states remain approximately equal, with an oscillatory behavior which features the characteristic period of the slow (torsional) modes ($T_{\text{torsion}} \sim 300$ fs). Superimposed is a weak oscillatory structure due to the fast (C=C stretch) modes ($T_{\text{stretch}} \sim 20$ fs). The dynamics apparently remains in a coherent regime over the observation period, and does not reach an equilibrium state.

The effective mode analysis as outlined above is expected to shed further light on the mechanism of the nonadiabatic decay of the XT state. Fig. 3 illustrates the results of wavepacket propagation for the successive orders $n = 0, \ldots, 2$ (i.e., 3 to 9 effective phonon modes) of the effective-mode hierarchy. These successive orders feature in alternation the high-frequency modes (for $n = 0$ and $n = 2$) and the low-frequency modes (for $n = 1$).[26]

Several observations can be inferred from Fig. 3: (i) At the order $n = 0$ (3 effective modes), i.e., for $\boldsymbol{H} = \boldsymbol{H}_{\text{eff}}$, no decay of the exciton state is observed. While the effective-mode construction guarantees that the very initial dynamics is correctly reproduced,[19] deviations from the exact dynamics occur from about 80 fs onwards. (ii) At the order $n = 1$ (6 effective modes), the XT $\to$ CT decay over the first 400 fs is correctly described. (iii) At the order $n = 2$ (9 effective modes), the dynamics is correctly reproduced over the entire time scale of observation (1.5 ps).
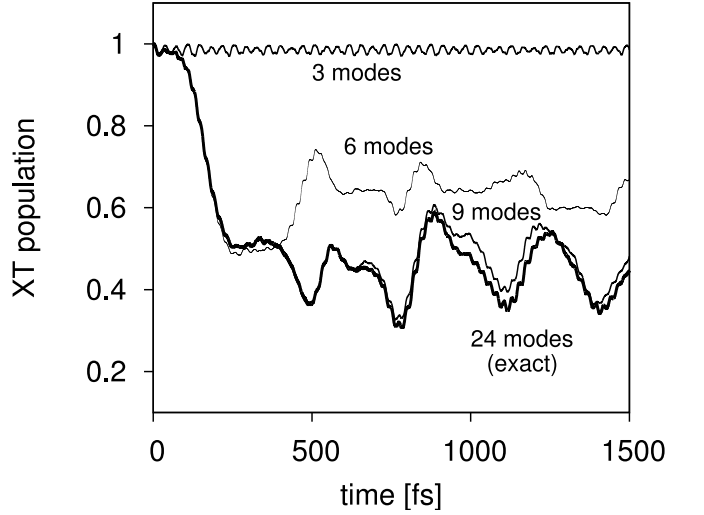

FIG. 3: Time-dependent population of the exciton (XT) diabatic state, from MCTDH calculations for the overall 24-mode system (bold line, labeled "exact") and the successive effective-mode approximations $\boldsymbol{H}^{(0)} = \boldsymbol{H}_{\text{eff}}$ (3 modes), $\boldsymbol{H}^{(1)}$ (6 modes), and $\boldsymbol{H}^{(2)}$ (9 modes), see Eqs. (5)-(6). Note that the 9-mode result is very close to the exact 24-mode calculation.

Strikingly, the presence of the high-frequency modes alone, at the level of the $n = 0$ description, does not account for the XT $\to$ CT transition. A more detailed analysis shows that the dynamics is characterized by oscillations between the adiabatic states, but the population essentially remains confined to the XT branch. The overall picture in the reduced 3-mode space is thus predominantly diabatic.

At the order $n = 1$ (6 effective modes), the low-frequency (torsional) branch of the phonon bath is added. As illustrated in Fig. 3, the initial XT state decay is now reproduced correctly. Apparently the low-frequency modes play a key role in the nonadiabatic dynamics, even though they do not directly couple to the electronic subsystem in the effective-mode picture. A study of the energy flow among the effective modes reveals that the low frequency modes act so as to dissipate the energy contained in the 3-mode (X_1, X_2, X_3) subspace, by an intramolecular vibrational redistribution (IVR) process.[26] In addition, the non-adiabatic dynamics as

such is influenced by the low-frequency components.

The next higher level, $n = 2$ (9 effective modes), yields very good agreement with the 24-mode reference calculation over the whole propagation period. The $\boldsymbol{H}^{(2)}$ approximation thus provides a suitable surrogate Hamiltonian on the time scale of observation.

Finally, Fig. 4 shows the time-dependent (X_1, X_2) position expectation values for the XT vs. CT portions of the wavepacket, from the 9-mode calculation. A concerted, oscillatory motion persists over the complete observation period. The comparatively regular behavior is consistent with repeated passages through a weakly avoided crossing region, rather than a direct passage through a conical intersection. The presence of the conical intersection space is essential, though, in that it defines the relevant nonadiabatic coupling region.

In summary, the present study emphasizes the role of coherent, quantum dynamical evolution, and its intrinsically multi-dimensional nature, in characterizing the nonadiabatic decay of the photochemically accessed XT state. Note that the presence of a high-dimensional intersection topology is not an exception, but rather the rule in multidimensional systems.[28, 31] The effective-mode analysis proposed here leads to a reduced dimensionality description, which provides important insight both from a static and a dynamical viewpoint. The representation of the potential in Fig. 2, in terms of the effective modes (X_1, X_2), yields a unique picture of the topology of the coupled electron-phonon system. From a dynamical point of view, the effective modes (X_1, X_2, X_3) determine the shortest, initial time scale, i.e., several tens of femtoseconds. For the present system, it is however essential to (at least partially) include the residual $(N - 3)$-mode phonon bath. As demonstrated in Fig. 3, a 9-mode representation yields a very good approximation of the overall 24-mode dynamics.

One of the main conclusions of this study is that the presence of the low-frequency (torsional) modes is a key element in the observed decay dynamics. Even though the high-frequency (C=C stretch) modes are most strongly coupled to the electronic subsystem, they do not by themselves induce the observed XT state decay. The coupling to the low-frequency phonon branch gives rise to an energy redistribution (IVR) which is essential in mediating the nonadiabatic decay. The importance of the low-frequency branch has been previously recognized in the context of the static absorption/emission spectroscopy of similar systems.[7, 32]

Our observations are in qualitative agreement with experimental results providing evidence for exciton regeneration at the TFB:F8BT heterojunction.[3, 13] Even though our calculations do not account for temperature effects, and the influence of dissipation is limited to the explicitly included phonon modes, we expect that the coherent, non-equilibrium nature of the dynamics remains a dominant feature over the first few picoseconds. Fur-
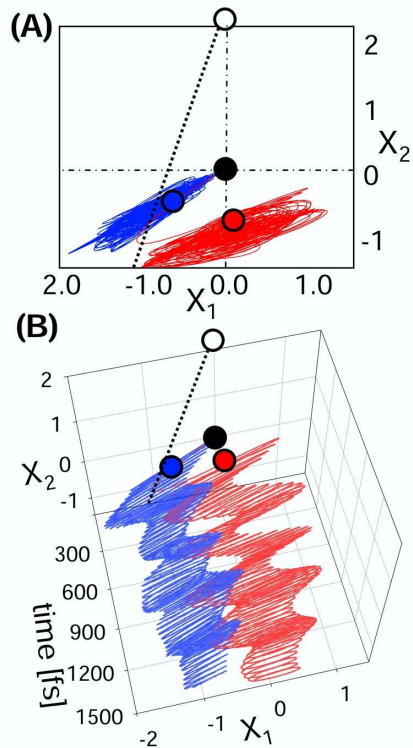

FIG. 4: (Color online) Time-dependent position expectation values of the XT (blue) and CT (red) portions of the wave-packet as a function of the branching plane coordinates (X_1, X_2), for the $n = 9$ calculation. The black, white, blue and red circles indicate the locations of the FC geometry, the conical intersection, and the XT vs. CT minima, respectively. The dashed line indicates the XT-CT avoided-crossing seam line. (A) Projection on the (X_1, X_2) plane and (B) 3-dimensional (X_1, X_2, t) plot.

ther studies including temperature effects will allow for a detailed comparison with the results, e.g., of the non-Markovian master equation calculations reported in Ref. [[14]].

[1] R. H. Friend, R. W. Gymer, A. B. Holmes, J. H. Burroughes, R. N. Marks, C. Taliani, D. D. C. Bradley, D. A. Dos Santos, J. L. Brédas, M. Lögdlund, and W. R. Salaneck, Nature **397**, 121 (1997).

[2] G. D. Scholes and G. Rumbles, Nature Materials **5**, 683 (2006).

[3] E. R. Bittner and J. Ramon, in *Quantum Dynamics of Complex Molecular Systems*, eds. I. Burghardt and D. A. Micha, Springer, Heidelberg, 2006.

[4] J. Ramon and E. R. Bittner, 2006, J. Phys. Chem. B., in press.

[5] E. R. Bittner, J. Ramon, and S. Karabunarliev, J. Chem. Phys. **122**, 214719 (2005).

[6] S. Karabunarliev and E. R. Bittner, J. Chem. Phys. **119**, 3988 (2003).

[7] S. Karabunarliev and E. R. Bittner, J. Chem. Phys. **118**, 4291 (2003).

[8] S. Karabunarliev, E. R. Bittner, and M. Baumgarten, J. Chem. Phys. **114**, 5863 (2001).

[9] G. Lanzani, G. Cerullo, C. Brabec, and N. S. Sacriftci, Phys. Rev. Lett. **90**, 047402 (2003).

[10] R. Kersting, U. Lemmer, R. F. Mahrt, K. Leo, H. Kurz, H. Bässler, and E. O. Göbel, Phys. Rev. Lett. **70**, 3820 (1993).

[11] P. Sreearunothai, A. C. Morteani, I. Avilov, J. Cornil, D. Beljonne, R. H. Friend, R. T. Phillips, C. Silva, and L. M. Herz, Phys. Rev. Lett. **96**, 117403 (2006).

[12] J. J. M. Halls, J. Cornil, D. A. dos Santos, R. Silbey, D.-H. Hwang, A. B. Holmes, J. L. Brédas, and R. H. Friend, Phys. Rev. B **60**, 5721 (1999).

[13] A. C. Morteani, P. Sreearunothai, L. M. Herz, R. H. Friend, and C. Silva, Phys. Rev. Lett. **92**, 247402 (2004).

[14] A. Pereverzev and E. R. Bittner, J. Chem. Phys. **125**, 104906 (2006).

[15] A. C. Morteani, A. S. Dhoot, J.-S. Kim, C. Silva, N. C. Greenham, C. Murphy, E. Moons, S. Cina, J. H. Burroughes and R. H. Friend, Adv. Mater. **15**, 1708 (2003).

[16] As a result, the overall photoluminescence efficiency of the TFB:F8BT blend is $\approx 60\%$ that of the pure F8BT, in spite of the presence of a heterojunction.

[17] L. S. Cederbaum, E. Gindensperger, and I. Burghardt, Phys. Rev. Lett. **94**, 113003 (2005).

[18] I. Burghardt, E. Gindensperger, and L. S. Cederbaum, Mol. Phys. **104**, 1081 (2006).

[19] E. Gindensperger, I. Burghardt, and L. S. Cederbaum, J. Chem. Phys. **124**, 144103 (2006).

[20] E. Gindensperger, I. Burghardt, and L. S. Cederbaum, J. Chem. Phys. **124**, 144104 (2006).

[21] I. Burghardt, in *Quantum Dynamics of Complex Molecular Systems*, eds. I. Burghardt and D. A. Micha, Springer, Heidelberg, 2006.

[22] H.-D. Meyer, U. Manthe, and L. S. Cederbaum, Chem. Phys. Lett. **165**, 73 (1990).

[23] U. Manthe, H.-D. Meyer, and L. S. Cederbaum, J. Chem. Phys. **97**, 3199 (1992).

[24] M. H. Beck, A. Jäckle, G. A. Worth, and H.-D. Meyer, Phys. Rep. **324**, 1 (2000).

[25] G. A. Worth, M. H. Beck, A. Jäckle, and H. Meyer, The MCTDH Package, Version 8.2 (2000); H.-D. Meyer, Version 8.3 (2002). See http://www.pci.uni-heidelberg.de/tc/usr/mctdh/.

[26] H. Tamura, E. R. Bittner, and I. Burghardt, 2006, in preparation.

[27] P. Grigolini and G. P. Parravicini, Phys. Rev. B **25**, 5180 (1982).

[28] H. Köppel, W. Domcke, and L. S. Cederbaum, Adv. Chem. Phys. **57**, 59 (1984).

[29] G. J. Atchity, S. S. Xantheas, and K. Ruedenberg, J. Chem. Phys. **95**, 1862 (1991).

[30] E. Gindensperger, H. Köppel, and L. S. Cederbaum, submitted to J. Chem. Phys.

[31] D. G. Truhlar and C. A. Mead, Phys. Rev. A **68**, 032501 (2003).

[32] S. Karabunarliev, M. Baumgarten, E. R. Bittner, and K. Müllen, J. Chem. Phys. **113**, 11372 (2000).